ELSEVIER

Journal of Power Sources 111 (2002) 210–220

JOURNAL OF POWER SOURCES

www.elsevier.com/locate/jpowsour

Performance study of commercial $LiCoO_2$ and spinel-based Li-ion cells

P. Ramadass, Bala Haran, Ralph White, Branko N. Popov*

Department of Chemical Engineering, University of South Carolina, Columbia, SC 29208, USA

Received 20 April 2002; accepted 29 April 2002

Abstract

The performance of Cell-Batt® Li-ion cells and Sony 18650 cells using non-stoichiometric spinel and $LiCoO_2$, respectively, as positive electrode material has been studied under several modes of charging. During cycling, the cells were opened at intermittent cycles and extensive material and electrochemical characterization was done on the active material at both electrodes. Capacity fade of spinel-based Li-ion cells was attributed to structural degradation at the cathode and loss of active material at both electrodes due to electrolyte oxidation. For the Sony cells both primary (Li^+) and secondary active material ($LiCoO_2$)/C) are lost during cycling.

Keywords: Li-ion cells; $LiCoO_2$; Cell-Batt®; Capacity fade; Sony 18650; Spinel

1. Introduction

One of the problems associated with the performance of Li-ion batteries is the capacity decay in the cell with cycling. This capacity fade is caused by various mechanisms, which depend on the electrode materials and also on the protocol adopted to charge the cell. Capacity fade in Li-ion cells can be attributed to unwanted side reactions that occur during overcharge or discharge, which causes electrolyte decomposition, passive film formation, active material dissolution and other phenomena [1–10].

Overcharging the Li-ion cells causes deposition of metallic Li on the negative electrode surface, which is a primary side reaction. Li deposition will take place in cells with excess cyclable Li due to either higher than desired initial mass ratio or lower than expected Li losses during the formation period [1]. According to Dahn and co-workers [2] and Aurbach and co-workers [3], the Li metal which is deposited on the negative electrode reacts quickly with the solvent or salt molecules in the vicinity giving Li_2CO_3, LiF or other products. The products formed may block the pores, leading to a loss of rate capability as well as capacity losses.

Dahn et al. [4] also mentioned that overcharging can lead to capacity loss due to inert material formation in the positive electrode (e.g. Co_3O_4 in case of $LiCoO_2$-based cells and Mn_2O_3 in case of spinel-based cells) and these final metal oxide products are inert to Li insertion/de-insertion and hence capacity is lost irreversibly. Formation of electrochemically inactive electrode decomposition products leads to a capacity imbalance between the electrodes.

Capacity loss during the formation period at the negative electrode was repeatedly characterized as an irreversible loss [5–8]. This loss is due to the formation of passive film formation over the surface of the electrode. Peled [5,6] explained many of the fundamental processes taking place at the Li and lithiated carbon electrode/electrolyte interfaces and developed mathematical models to explain these interfacial phenomena. The interfacial films are composed of reaction products, such as Li_2CO_3 and LiF resulting from electrolyte (salt/solvent) reduction and also due to Li-ion reduction [8]. The initial loss of Li-ions in forming this film causes the capacity balance between the two electrodes to change, that ultimately results in diminished utilization and hence a decreased specific energy for the entire battery. The solid/electrolyte interface (SEI) passivation layer on the negative electrode surface plays a major role in determining the electrode battery behavior and properties including cycle life, shelf life and irreversible capacity loss.

Apart from losses due to overcharging and film formation, capacity fade in positive electrode can also occur due to active material dissolution. Thackeray and co-workers [9] was the first to mention dissolution of Mn to be one of the

* Corresponding author. Tel.: +1-803-777-7314; fax: +1-803-777-8265.
E-mail address: popov@engr.sc.edu (B.N. Popov).

0378-7753/02/$ – see front matter
PII: S0378-7753(02)00267-7

reason for capacity fade with cycling in case of spinel-based Li-ion cells. Tarascon et al. [10] detected the presence of Mn on the surface of negative electrode by Rutherford back-scattering spectroscopy (RBS). Wen et al. [11] reported that the capacity fade on cycling in the higher voltage region was attributed to the fact that the active electrode material was gradually converted to a lower voltage defect spinel phase via the dissolution of Mn into the electrolyte. To summarize, the factors determining positive electrode dissolution are structural defects in the positive active material, high charging potentials and the carbon content in the composite positive electrode [12–14].

Since most of the capacity fade studies done previously were based on either positive or negative single electrodes, in this work we studied the performance of commercially available Li-ion cells. Our previous capacity fade studies [15,16] indicated that the charging protocol significantly influences the capacity loss of with cycling. In this paper, the performance of Sony 18650, $LiCoO_2$-based cells were compared with the performance of Cell-Batt®, $LiMn_2O_4$-based cells using constant current–constant voltage (CC–CV) mode of charging. The performance of Cell-Batt® cells was also studied by charging the battery to several cut-off potentials with a single applied current. The Cell-Batt® batteries were also charged potentiostatically, using CV charging mode.

2. Experimental

2.1. Full-cell studies

Cell-Batt® Li-ion cells (obtained from International Battery Technologies) with a rated capacity of 1050 mAh were used to study the performance under various charging modes. Table 1 summarizes the characteristics of the Cell-Batt® cell. The charging protocol used was CC–CV protocol, where the cells were charged at a CC of 1 A to end to cut-off voltage in the range between 4 and 4.3 V and subsequently the cells were charged potentiostatically until the current decays to 50 mA. Arbin BT 2000 cycler has been used for all cycling studies. Cycle life studies using this mode of charging were carried out up to 100 cycles.

CC–CV protocol with different charging currents to one end potential was a other mode for charging the batteries

Table 1
Physical characteristics of Cell-Batt® Li-ion battery electrodes

Characteristics	Positive spinel	Negative carbon
Mass of the electrode material (g)	9.592	5.087
Geometric area (both sides) (cm^2)	436	498
Loading on one side (mg/cm^2)	22	10.2
Thickness of the electrode (μm)	91	70
Dimensions of the electrode (cm × cm)	54.5 × 4	58.5 × 4

Table 2
Physical characteristics of Sony 18650 cell electrodes

Characteristics	$LiCoO_2$	Carbon
Mass of the electrode material (g)	13.4	5.7
Geometric area for both sides (cm^2)	531	603
Loading on one side (mg/cm^2)	28.4	11.9
Thickness of the electrode (mm)	183	193
Dimensions of the electrode (cm × cm)	48.3 × 5.5	52.9 × 5.7

In this case, the cycle life studies were carried out up to 800 cycles. The Sony cells were charged using the CC–CV protocol as follows: the batteries were charge using CC of 1 A until the voltage reaches 4.2 V and subsequently the cells were charged potentiostatically at 4.2 V until the current drops to 50 mA (Table 2).

Impedance studies were made for the full-cells at several cycles and rate capability measurements were done for the Sony cells after various cycles (1, 150, 300 and 800 cycles). Solartron SI 1255 HF frequency response analyzer and potentiostat/galvanostat model 273A were used for the electrochemical characterization studies. The cycling studies were carried out using Arbin charger.

2.2. Half-cell studies

Half-cell studies were done to determine the extent of capacity loss in individual electrodes. The can of fresh or cycled cells was carefully opened at fully discharged state in a glove box filled with ultrapure argon (National Gas and Welders Inc.). The term ‘‘fresh electrode’’ refers to the electrode of the Cell-Batt®/Sony battery when it is bought. The commercial cells are already pre-conditioned before reaching the market. Hence, the irreversible capacity loss in the negative electrode was taken care while pre-conditioning itself.

Next, pellet electrodes were made from the positive and negative electrodes and were used as working electrodes in the T-cell. Pure Li metal was used as the counter and reference electrode.

The diameter of the pellet electrodes was 1.2 cm and ratio of area of the disc electrode to original electrode area was 0.00243. $LiPF_6$ (1 M) was used as the electrolyte in a 1:1 mixture of ethylene carbonate (EC) and dimethyl carbonate (DMC). EIS studies were done on the T-cells to understand the influence of positive and negative electrode on total impedance of the cell. XRD and EDAX measurements were also done on the cycled electrode materials.

3. Results and discussion

3.1. Capacity fade in spinel-based Cell-Batt® cells

The positive electrode used in the Cell-Batt® cell is a non-stoichiometric spinel and the negative electrode is carbon. In

general, copper and aluminum are used as current collectors for negative and positive electrodes, respectively. Hence, a typical electrochemical Li-ion cell can be represented as $Cu|Li_xC|Li^+|Li_\alpha(Mn_{2-\gamma}Li_\gamma)O_4|Al$. At the negative electrode of the Li-ion cell the following electrochemical reaction occurs:

$$Li_xC + \delta Li^+ + \delta e^- \underset{\text{discharge}}{\overset{\text{charge}}{\rightleftarrows}} Li_{x+\delta}C \quad (1)$$

while at the positive electrode the reaction is:

$$Li_\alpha(Mn_{2-\gamma}Li_\gamma)O_4 \underset{\text{discharge}}{\overset{\text{charge}}{\rightleftarrows}} Li_{\alpha-\delta}(Mn_{2-\gamma}Li_\gamma)O_4 + \delta Li^+ + \delta e^- \quad (2)$$

During charge Li^+ intercalates into the carbon electrode (reduction) and the anode potential moves closer to 0 from 1.2 V. Simultaneously, spinel is oxidized (de-intercalation) and its potential changes from 3 to 4.2 V. During discharge, the reverse of the above occurs. The extent to which Li-ion is intercalated into or de-intercalated from electrode materials is in general expressed in terms of state of charge (SOC).

The charge curves showed in Fig. 1a represent both CC and CV parts of the CC–CV charging mode. As shown in this figure, the cell voltage varies with time or the capacity during charging the cell at CC. The charge curve also shows the variation or a decay of charging current, when the cell was charged in the CV mode. Since charging and discharging processes in a typical Li-ion cells represents the Li intercalation and de-intercalation between the positive and negative electrodes which is diffusion limited process, sufficient time has to be given to the cell for complete charging.

The charge time of all Li-ion batteries, when charged at a 1*C* initial current, is about 3 h. Full charge is attained after the voltage has reached the upper voltage threshold and the current has dropped and leveled off at about 3% of the nominal charge current. Thus, we adopt a CC–CV protocol for charging the Li-ion cell where instead of fixing the total charging time (CC + CV time) the charging will be stopped when the current decays to about 50 mA during the CV mode of charging. Fig. 1b shows a typical 1*C* discharge curve of a Li-ion cell with $LiMn_2O_4$ as the positive electrode material.

One of the main reasons for capacity fade in Li-ion cells is overcharging the cell. Li-ion batteries operate safely within their normal operating voltage. However, they become increasingly unstable if charged to higher voltages. Above 4.3 V, Li metal deposits on the anode. In addition, the cathode material becomes an oxidizing agent, loses stability and releases oxygen. Overcharging also causes the cell to heat up. According to Aurbach et al. [17], the onset of electrolyte oxidation in Li-ion cells may be as low as 3.7 V. This oxidation of the solution produces a sufficient concentration of Lewis acids, which interact with the active mass and lead to its partial dissolution. Acid generation leads to Mn disproportionation and dissolution in the electrolyte

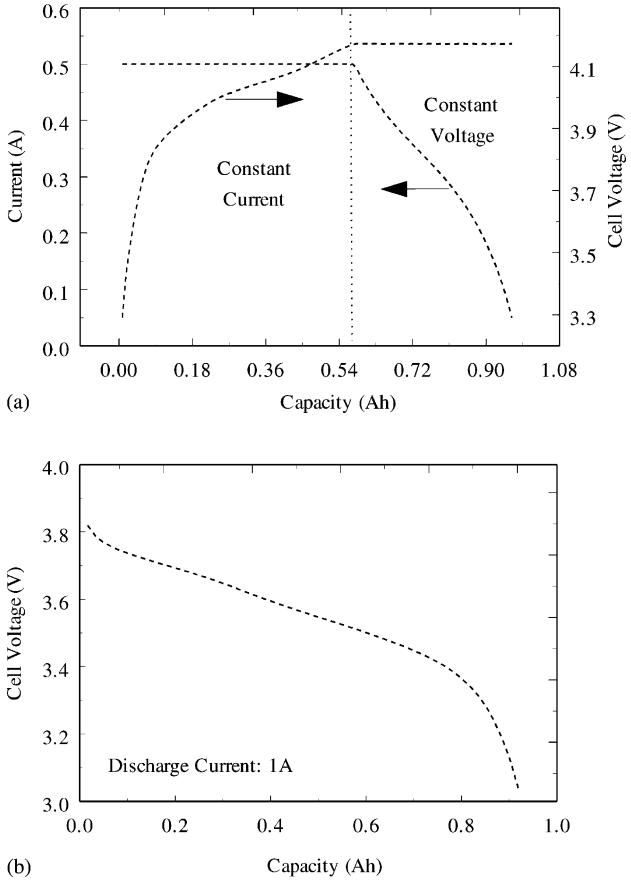

Fig. 1. A typical charge (a) and discharge (b) curve of a 1 Ah Cell-Batt® Li-ion cell.

during normal cycling. Since, electrolyte oxidation starts at 3.7 V, the amount of oxidation products generated depends on the charge current and the charging time.

In order to analyze, how the charging influences the performance of Li-ion cells, we cycled the cells using different modes of charging. The objective was to determine which cut-off potential would reduce the overcharging of the battery. Fig. 2 presents the charge curves of the first cycle for the Cell-Batt® cells which were charged to five different cut-off potentials namely 4, 4.05, 4.1, 4.17 and 4.3 V using CC–CV protocol. Each cell was charged to one particular cut-off value during the CC part of charging with a dc current of 1 A, followed by a CV charging until the charging current decays to 50 mA. The discharge current used for all cells was 1 A.

The plot clearly shows the charging utilization, when the cell is in CC mode as well as in CV mode. The term utilization denotes the ratio between the observed capacities to the rated capacity of the cell. The cell charged to 4 V using the CC–CV protocol gave only 50% utilization and as expected it increases with the increase of the end potential. As shown in Fig. 2, the CC charging time is very less, when the cell was charged to lower values of end potentials. At lower end potential, almost the entire charging was done in CV mode. The observed results can be explained by taking

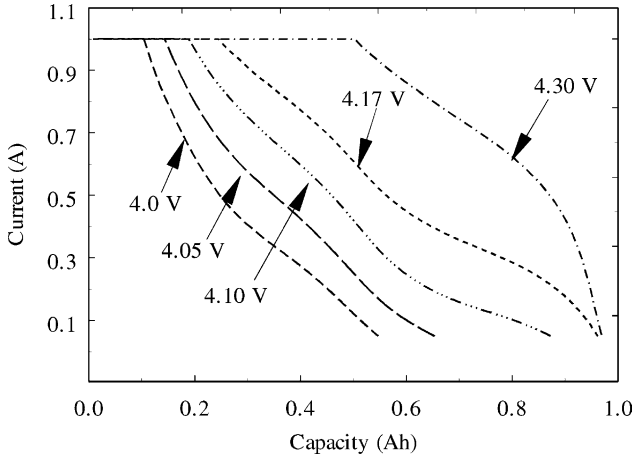

Fig. 2. Charge curves of Cell-Batt® cells for the first cycle when charge to different end potentials.

into account the fact that for a given value of charging current (∼1 A), it takes lesser time for the cell to reach lower cut-off potentials, such as 4 or 4.05 V when compared to the time necessary to reach 4.17 or 4.3 V.

The CC charging time, the CV charging time and the total charging time of the cells charged to different cut-off voltages is presented in Table 3. The open circuit voltage of the cell in the discharged state is around 3 V. It can be seen from the table that most part of the charging takes place in CV mode when we charge the cells at lower cut-off potentials (4, 4.05 and 4.1 V). The total charging time for the cell charged to 4.3 V is smaller when compared with that of 4.17 V.

The capacity increases with increase in end potential used for charging the cell. Increasing the cut-off voltage to 4.17 V resulted in a completely charged cell. A maximum capacity

Table 3
Comparison of charging time for Li-ion cells charged to different cut-off voltages

Cut-off voltage (V)	Charging time (h)			Capacity fade after 100 cycles (%)
	CC time	CV time	Total time	
4.00	0.09	1.74	1.83	2.20
4.05	0.13	2.08	2.21	3.60
4.10	0.17	3.04	3.21	4.02
4.17	0.24	2.08	2.32	4.95
4.30	0.49	0.92	1.41	6.00

was observed for the cell charged to 4.17 V. There is no further increase in capacity when the cell is charged beyond 4.17 V. Note that the efficiency (a ratio of charge to discharge capacities) remains close to 100%. The maximum capacity fade after 100 cycles of 6% was observed for the cell charged to end potential of 4.3 V. These results provide important information with regard to estimation of an optimum cut-off potential for charging the cell that maximizes the capacity while avoiding overcharging the cell.

Fig. 3 shows the performance of the cells charged to different end potentials for the first 100 cycles. It is clear from this figure that the cell charged to end potentials, namely 4 and 4.05 V, nearly showed almost the same performance for the entire 100 cycles and the capacity fade is <5%.

Fig. 4a presents the charge curves obtained by charging the Cell-Batt® cells at four discharge different currents to a cut-off potential of 4.17 V. The batteries were charged using the following charging currents: 0.25, 0.5, 0.75 and 1 A. At 0.25 A, almost 80% of the charging was done in the CC mode, followed by a CV charging. When higher charging currents, such as 1 A were used only 25% of the charging

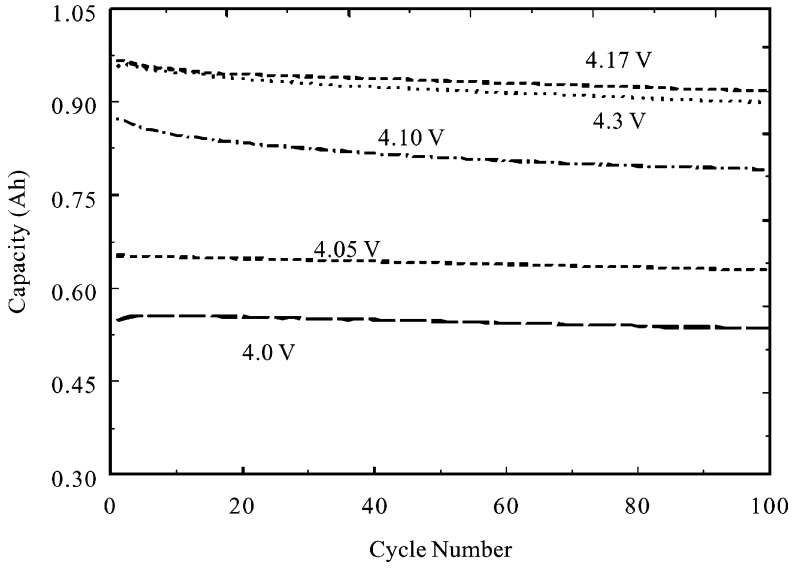

Fig. 3. Capacity fade of Li-ion cells for 100 cycles when charged for different end potentials.

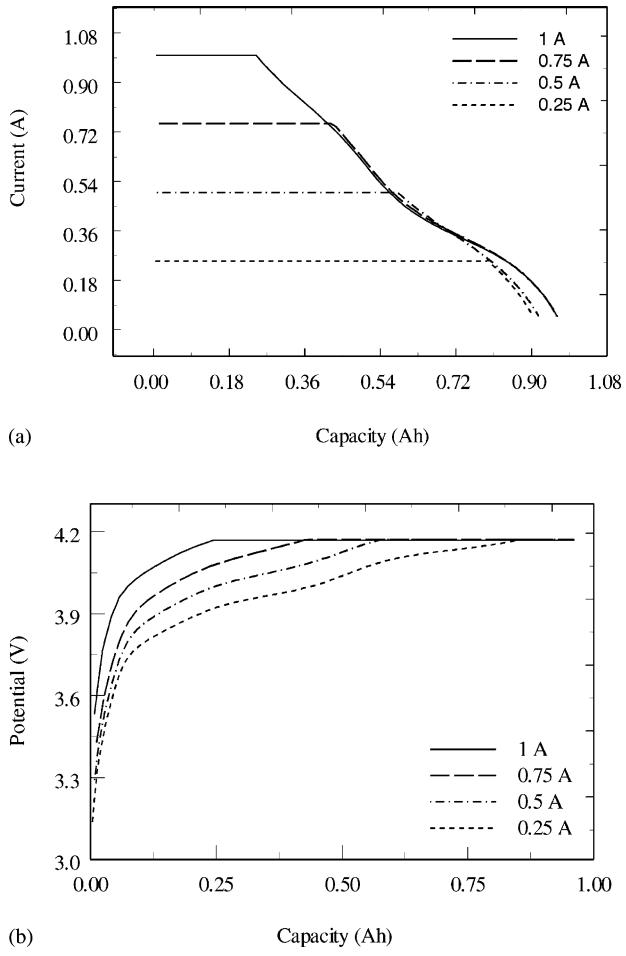

Fig. 4. Change in current (a) and potential (b) with capacity at different charge rates.

was done in the CC mode. In general for all charge currents used in this study, the CC charging time decreases with increase in charging rate. In other words, increasing the charging currents results the battery to be charged in a CV mode during most part of the charge.

Increasing the charge current increases the Li depletion rate from the surface of the negative electrode resulting in ore Li-ions to be transferred to the positive electrode. Since the positive potential is controlled by the amount of intercalated Li, due to a slow mass transfer of Li-ions into the bulk of the active material, the surface saturation with Li and thus the cut-off voltage will be reached faster at higher current densities. Thus, one can expect the CC time to decrease and CV time to increase by increasing the charging current from 0.25 to 1 A. The current decay during charging the cell in CV mode was similar for all charging rates.

Fig. 4b shows how the cell potential varies with capacity for different charging currents. The cell reaches the cut-off value of 4.17 V faster, when charged at higher currents, such as 0.75 or 1 A. The total charging time as a function of cycle life is given in Table 4. It is evident that the total charging

Table 4
Change in total charging time with cycling at different charge rates

Cycle number	Total charging time (h)			
	0.25 A	0.5 A	0.75 A	1 A
1	3.92	2.72	2.46	2.32
100	3.91	2.69	2.46	2.26
200	3.91	2.67	2.32	2.14
300	3.90	2.64	2.32	2.11
400	3.90	2.61	2.30	2.07
500	3.83	2.46	2.28	2.07

time (CC + CV time) is higher for cells cycled at lower currents. However, increasing the charging rate above 0.5 A does not decrease the total time significantly. For all three currents (0.5, 0.75 and 1 A), the CC and CV times vary significantly. This can lead to differing capacities with cycling. Fig. 5 presents the discharge curves obtained for Cell-Batt® cell corresponding to cycle numbers 1 and 500. The cell was charged with a CC of 0.75 A. The cut-off discharge voltage was set at 3 V. The discharge current is 1 A. Fig. 5 clearly indicates a capacity fade as well as the drop in the cell voltage with cycling.

Table 5 gives the percentage capacity losses of the Cell-Batt® cells cycled at the four different charging rated for various cycle numbers. The cell charged at 0.5 A showed a capacity fade of about 15.4% after 800 cycles, while for the cell charged with 1 A current the capacity fade showed the highest value of 19%. The performance of the cells charged with 0.25 and 0.75 A current fall between these two ranges. The total charging time for different charging currents decreases with cycling, which was expected since the capacity of the cell decays continuously.

Capacity fade of spinel electrodes as well as carbon anodes has been extensively studied in the literature [20]. Gummow et al. [9] found that the capacity fading of spinel is due to the dissolution of Mn into the electrolyte solution. Xia

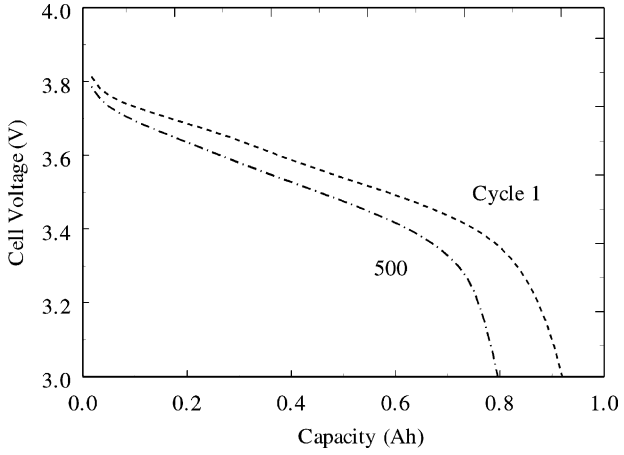

Fig. 5. Discharge curves of Cell-Batt® cell for cycles 1 and 500 for a charging current of 0.75 A.

Table 5
Discharge capacities and percentage capacity fade of Cell-Batt® cells for 800 cycles charged at different rates

Cycle number	Capacity fade (%)			
	0.25*C*	0.5*C*	0.75*C*	1*C*
100	3.64	4.09	4.49	4.30
150	8.31	8.43	8.69	8.67
300	10.11	9.88	10.23	10.08
500	12.95	12.51	12.99	13.45
800	17.10	15.40	18.20	19.00

et al. [14] attributed the capacity fade of spinel-based Li-ion battery to transformation of unstable two-phase spinel to a more stable one-phase structure via loss of MnO. Huang et al. [19] have correlated the capacity loss of stoichiometric and non-stoichiometric spinel to electrode structural integrity. Capacity fade could be also due to loss of active material because of formation of oxidation products at the particle/electrolyte interface. This oxidation process of the solution produces a sufficient concentration of Lewis acids, which interact with the active mass and lead to its partial dissolution. The generation of Lewis acids has been observed irrespective of the type of cathode used [18]. Acid generation leads to Mn disproportionation and dissolution in the electrolyte during normal cycling. As the electrode is kept for longer periods of time at 4.17 V at higher charge rates (>0.5 A), this could cause more oxidation of the electrolyte. For the same reason, at a given charge rate increasing the end-of-charge voltage causes more capacity fade.

Impedance measurements were done for both full-cells and also for the individual electrodes taken form the cells after various charge discharge cycles to observe whether there is an increase in resistance with cycling that could be related to capacity fade with cycling. Impedance studies were first done for a fresh cell to see the variation of overall cell resistance with respect to SOC. It was found that the cell impedance decreases with increase in SOC. This is an expected feature of Li-ion cell since during charge, Li de-intercalates from positive electrode, thereby increasing its conductivity. Transition metal oxide by itself acts as a good conductor. Li intercalation through the interstitial sites of the transition metal oxide makes it semi-conductive. It is the other way for negative electrode where Li intercalation into carbon increases its conductivity.

Impedance studies were done for fresh as well as for the cycled cells. Fig. 6 presents the cell impedance of the 0.5 A charged battery at different cycles. In this plot, a comparison is made between the impedance of fresh cell and the cells cycled 400 and 800 times at 0 and 100 SOC. Impedance results show a slight increase in cell impedance with cycling for both SOCs. Since impedance studies of a full-cell gives only the overall cell resistance, the contribution of positive and negative electrode resistance to the overall cell impedance cannot be found out unless half-cell studies were made for individual electrodes.

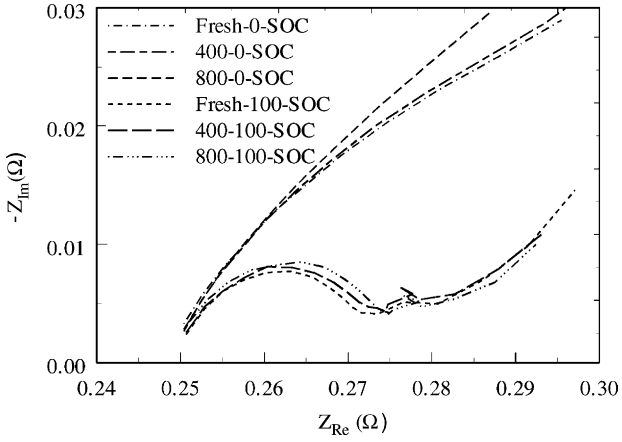

Fig. 6. Variation in total cell impedance of Cell-Batt®® battery at different charge/discharge cycles. The cell was charged at 0.5 A.

Similar EIS studies were also done for the individual electrodes using the T-cell assembly with Li foil as both reference and counter electrodes. The impedance measurements for individual electrodes in their discharged state indicated that the overall resistance of the carbon electrode is slightly larger than that of the spinel. With continuous cycling there is no significant change in the overall impedance for both the electrodes.

Since the resistance change at both electrodes are negligible, the capacity loss arises due to loss of active material. The loss of active material may result from: (a) loss of active Li^+ due to side reactions; and/or (b) loss of secondary active material spinel or carbon. The loss of spinel or carbon means that a part of the electrode material may undergo a phase transformation or structural degradation that causes decrease in lithiation efficiency and thus with cycling the secondary active material can lose its capacity to fully intercalate Li^+.

To investigate this phenomenon, materials from both electrodes were analyzed separately in T-cells. In these experiments, we used Li foil as both counter and reference electrodes. Any loss in capacity as compared to material from the fresh cell can be clearly attributed to loss in lithiation capacity of individual electrodes.

For the spinel electrode taken from a fresh battery de-lithiation for 14 h at 10 mA/g gives a capacity of 140 mAh/g. These results were compared with spinel active material from a cell cycled 800 times. In this case, de-lithiation for 15.3 h at 7.84 mA/g gives a capacity of 120 mAh/g. Similar capacity losses were observed for the carbon electrode also where after 800 cycles a decrease in the specific capacity from 255 to 225 mAh/g.

Since lithiation and de-lithiation steps are limited by diffusion, these studies were carried out at very low currents in order to reach a completely lithiated or de-lithiated state and to make a comparison of results between fresh and cycled electrodes. This study clearly indicated that part of the capacity fade could be attributed to the change in

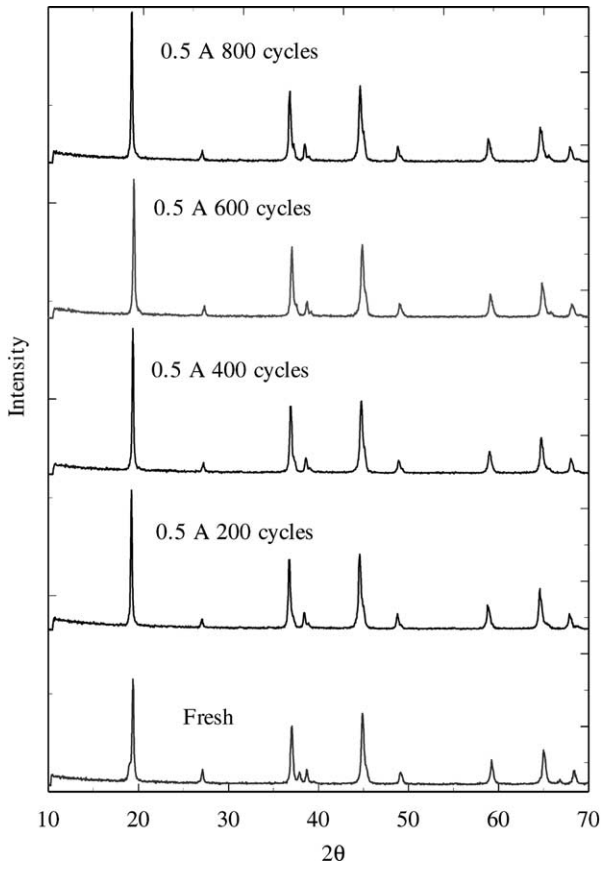

Fig. 7. XRD patterns of spinel after different charge/discharge cycles. $LiMn_2O_4$ was taken from Cell-Batt® battery charged at 0.5 A.

lithiation capacity of the individual electrodes. To analyze this in more detail, changes in electrode structure with cycling were studied using XRD and EDAX analysis.

Fig. 7 presents the XRD patterns of the spinel samples taken out of the Cell-Batt® battery charged at 0.5 A at different cycles and compared with the XRD pattern of the fresh sample. The patterns were collected at the end of discharge with a Tigaku 405S5 X-ray diffractometer using Cu Kα radiation. With cycling, additional phases of Li–Mn compounds are seen in the diffraction patterns. The spinel peaks shift slightly to the right that indicates a contraction in the lattice parameter. On analyzing the XRD patterns of the electrode that were charged and discharged for several cycles, we noticed that apart from the non-stoichiometric spinel phase, an additional phase slowly starts accumulating with cycling. This could be due to formation of defect spinel product λ-MnO_2 according to the chemical reaction as proposed by Hunter [21]:

$$2LiMn_2O_4 \rightarrow 3\lambda\text{-}MnO_2(\text{solid}) + MnO(\text{solution}) + Li_2O(\text{solution}) \quad (3)$$

The valence state of Mn in λ-MnO_2 is +4 while that of non-stoichiometric spinel its valence state is +3. It was known that the ionic radii of Mn^{4+} is less than that of Mn^{3+} and hence with the slow accumulation of the λ-MnO_2 phase, the lattice shrinks which was estimated by means of the shift of (4 4 0)-diffraction peak towards higher diffraction angles. The lattice constant '*a*' was found to decrease from 8.17 to 8.13 Å.

EDAX analysis was made for the negative electrode taken from the cells after several charge discharge cycles to look for any presence of MnO that could have dissolved in the solution. Analysis of the samples taken from the cycled cells reveals the presence of Mn over the surface of carbon and the Mn content was found to increase with cycling. Although, EDAX is qualitative in nature the presence of Mn on the carbon surface indicates Mn dissolution due to electrolyte oxidation during charge and deposition on the anode during subsequent cycles. The MnO dissolved in the solution is deposited on the carbon anode. This was confirmed by EDAX analysis for the carbon samples taken after different charge/discharge cycles. Up to 200 cycles, the presence of Mn over the surface of carbon is very negligible. However, from the EDAX analysis of the samples taken after several cycles, it can be seen that the Mn content increases with cycling. Although, EDAX is qualitative in nature the presence of Mn on the carbon surface indicates Mn dissolution due to electrolyte oxidation during charge and deposition on the anode during subsequent cycles. The acid generated during electrolyte oxidation could attack the SEI film formed on the carbon surface, which is attributed to capacity loss due to secondary active material degradation of negative electrode.

To summarize, impedance studies on spinel-based Li-ion cells show no significant increase in resistance at both electrodes after 800 charge/discharge cycles. XRD studies of spinel electrode reveal the formation of an additional phase (λ-MnO_2) with cycling that leads to dissolution of Mn in the electrolyte. Mn dissolution is also attributed to acid generated due to electrolyte oxidation during charge. The generated acid also attacks the SEI layer and leads to loss of active material at the anode. Hence, capacity fade of the spinel-based Li-ion cells can be attributed to: (i) structural degradation at the cathode; and (ii) loss of active materials at both electrodes due to electrolyte oxidation.

3.2. Capacity fade of Sony 18650 cells with $LiCoO_2$ as positive electrode

The rated capacity of Sony 18650 cell is 1.8 Ah. The intercalation and de-intercalation steps that occur during charge and discharge of the Sony 18650 cell can be represented similar to that of the Cell-Batt® cell. At the negative electrode of the Sony 18650 cell the following electrochemical reaction occurs, which is the same as that of the Cell-Batt® cell (Eq. (1)), while at the positive electrode the reaction is:

$$Li_yCoO_2 \underset{\text{discharge}}{\overset{\text{charge}}{\rightleftarrows}} Li_{y-\delta}CoO_2 + \delta Li^+ + \delta e^- \quad (4)$$

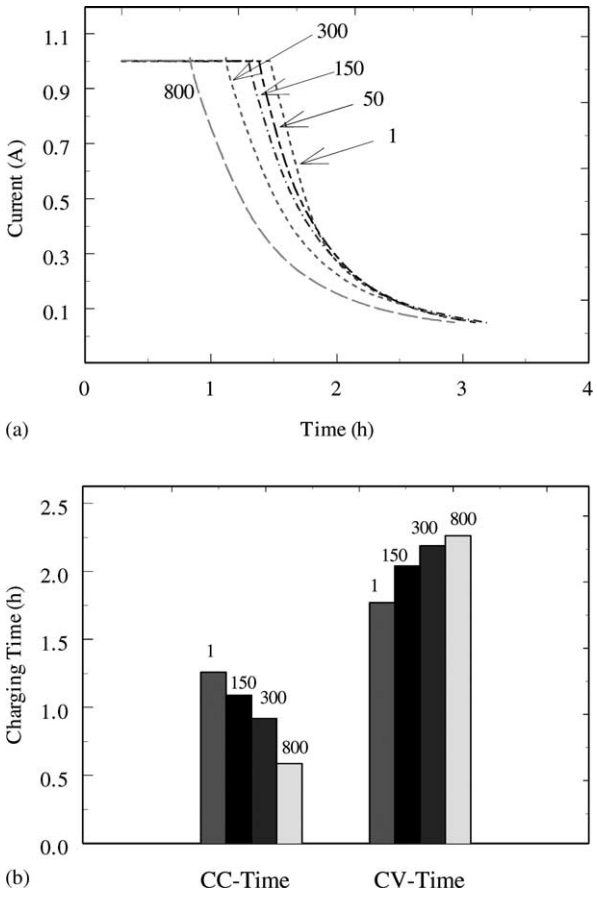

Fig. 8. (a) Charge curves for Sony 18650 cell for several cycles; (b) CC and CV charging times for Sony 18650 cells for 800 cycles.

The cells were charged using CC–CV protocol by using a CC of 1 A until the cell potential reaches its cut-off value of 4.2 V followed by CV charging until the current decays to 50 mA. The cells were discharged with a CC of 1 A up to a voltage cut-off value of 2.5 V. For this study, we chose the Sony cells of 1.8 Ah rated capacity from the battery pack that is being used to power the camcorders.

Fig. 8a shows the variation of CC charging time and CV charging time as a function of number of cycles. The CC time for the first cycle was found to be about 1.29 h when charged with a CC of 1 A and decreases continuously with cycling becoming 35 min at the end of 800 cycles. The exact times estimated during cycling are presented as bar plots shown in Fig. 8b. This figure clearly indicates a decrease in CC time and increase in CV time with cycling. This is quite in contrast with the results observed for Cell-Batt® cells where both CC and CV time continues to decrease with cycling which contributes the total charging time to decrease with cycling. The total charging time remains almost constant for Sony 18650 cells.

The discharge curves obtained of Sony 18650 cells as a function of number of cycles are shown in Fig. 9. As shown in this figure, all cells showed a drop in potential during the earlier stages of discharge, which increases with cycling. After 800 cycles the capacity loss was found to be about

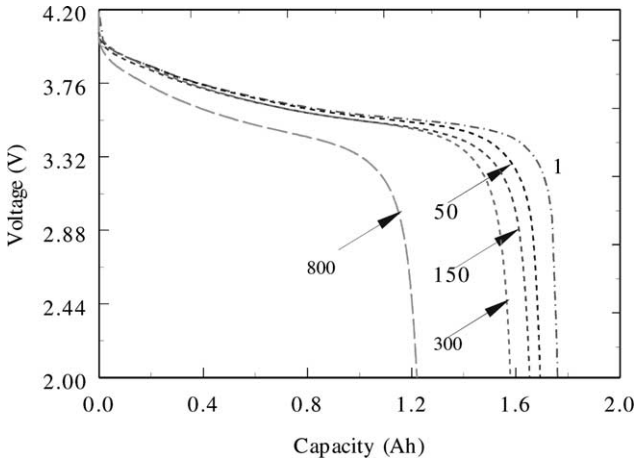

Fig. 9. Discharge curves of Sony 18650 cells for various cycles.

Table 6
Discharge capacities and percentage capacity fade of Sony 18650 cells for 800 cycles of charge and discharge

Cycle number	Discharge capacity (Ah)	Capacity fade (%)
1	1.7601	
50	1.6937	3.80
100	1.6700	5.11
150	1.6529	6.09
300	1.5790	10.29
500	1.3640	22.50
800	1.2210	30.63

30%. Table 6 shows the values of the capacity fade for different cycles. The variation of discharge capacity and the variation of CC charging time with cycle number are shown in Fig. 10. The results indicated that the capacity fade rate is higher for the first 100 cycles when compared with the subsequent cycles. Capacity loss after 100 cycles varies almost linear with cycle number. This is in close coincidence with the variation of CC charging time with cycle number.

Fig. 11 presents the comparison of rate capability of Sony 18650 cells for various cycles with that of fresh one. Rate

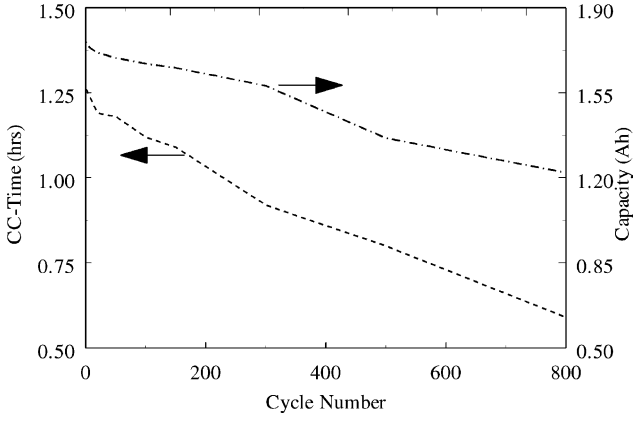

Fig. 10. Variation of CC charging time and discharge capacity with cycle number for Sony 18650 cells.

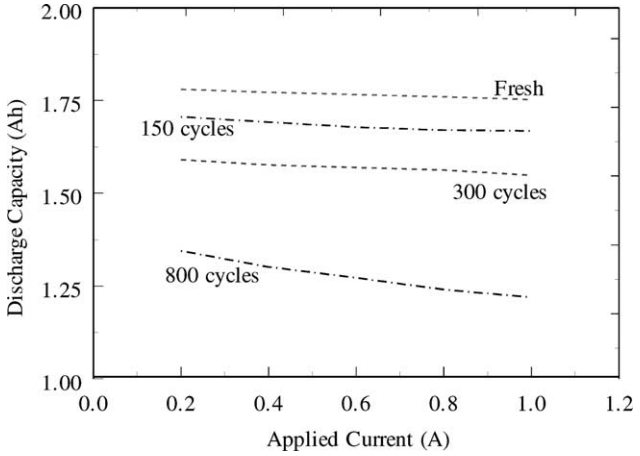

Fig. 11. Rate capability studies for the Sony 18650 cells cycled 800 times.

capability tests were done by charging the cells using the CC–CV protocol. The charging current during the CC portion was held constant at 1 A in all studies. Subsequent to charging, the cells were discharged galvanostatically at five different currents, namely 0.2, 0.4, 0.6, 0.8 and 1 A. Initially a small decay in capacity is seen with increase in discharge current. With increased cycling, the plot shows poor performance for cells discharged with higher currents. The rate capability measurements at the end of 800 cycles show a clear gradation in the performance of the cell with respect to applied current for discharging it. These results indicate that the cell resistance increases with cycling contributing to a poor utilization at higher discharge rates.

Fig. 12 presents the Nyquist plots of fully charged Sony 18650 cells cycled at RT during first cycle and after 800 cycles. As shown in this figure, the overall cell resistance increases with cycling. The cell cycled 800 times showed a large increase in the overall resistance when compared with that of fresh one. There was also a slight increase in the electrolyte resistance with cycling from 0.31 Ω during the first cycle to 0.36 Ω after 800 cycles of charge and discharge. Impedance measurements were also made for completely discharged cells and the increase in the overall cell resistance was found to be similar. The impedance results observed for Sony cell were different from those obtained for Cell-Batt® cells. The Cell-Batt® cells showed only a slight increase in impedance with cycling at both charged and discharged states. The observed increase in cell resistance in case of Sony batteries indicates a change in resistance of the individual cell components due to formation of less conductive oxide layers on the electrodes.

Impedance measurements were next performed for both positive and negative electrodes taken from fresh cell as well as from the cells cycled 150, 300 and 800 times. The measurements were carried out in both lithiated and de-lithiated states for both the electrodes. The shape of the Nyquist plots does not change very much with cycling. However, the size of the semicircles increases drastically indicating a continuous increase in electrode resistances with cycling. The bar plots shown in Fig. 13 gives the variation of both positive and negative electrode resistances for different cycles. The resistances of both positive and negative electrodes increase with cycling with the positive electrode resistance being always greater than that of the negative during the entire period of charge and discharge. Impedance results of individual electrodes indicated that Cell-Batt® cells showed only a slight increase in resistance for both spinel and carbon electrode resistance and overall, the resistance of carbon electrode was found to be higher than that of the spinel.

To determine which component of the battery contributes most to the capacity fade, T-cell studies were carried out for both positive and negative electrodes. Pellet electrodes from the cells after different cycles were cycled at low rates and the electrode capacity was determined. The results are presented in Table 7. For $LiCoO_2$, a CC of 7.78 mA/g was used for both to charge and to discharge the cell. The $LiCoO_2$ pellet taken from the fresh cell was charged for approximately 18 h. Similar studies were also done on the carbon electrode by using a charging current of 11.14 mA/g. The low rate was used in this study in order to eliminate any effects (a decrease of rate capability) arising

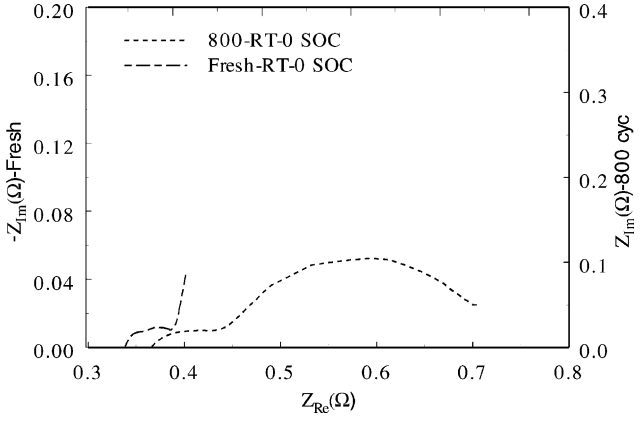

Fig. 12. Nyquist plots for a fully discharged Sony 18650 cell after cycles 1 and 800.

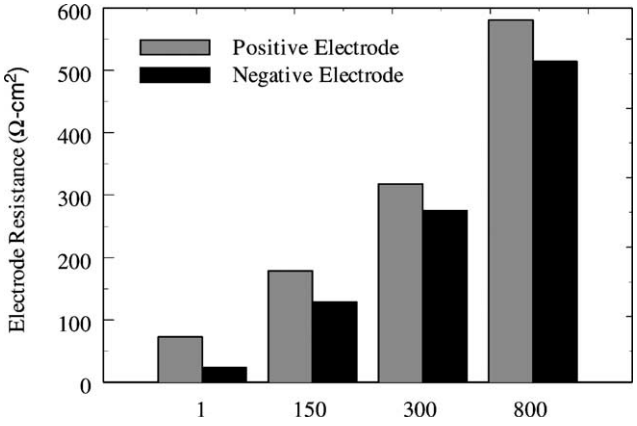

Fig. 13. Variation of positive and negative electrode resistances of Sony 18650 cell during cycling.

Table 7
Specific capacity of positive and negative electrodes at various cycle numbers

Cycle number	Specific capacity (mAh/g)	
	$LiCoO_2$	Carbon
1	147.81	306.17
150	144.29	299.55
300	139.17	283.95
800	121.23	225.21

due to electrode resistance. Since the studies were done with Li^+ foil as the counter electrode there are no capacity limitations due to the other electrode. Further, use of fresh electrolyte eliminates any losses arising due to the electrolyte evaporation in the battery. Hence, using this set-up and studying $LiCoO_2$/C from cells at different cycles, our goal was to analyze the losses from the secondary active material $LiCoO_2$/C electrode alone. Comparing the data obtained from T-cells to those obtained from the full-cell, it was possible to differentiate the capacity loss from the primary active material, Li^+, and the capacity loss resulting from a loss of a secondary active material, $LiCoO_2$/C.

As shown in Table 7, $LiCoO_2$ from the fresh battery has a capacity of 148 mAh/g. The capacity in this case was normalized to the total weight of the pellet, which includes binder and other additives minus the weight of the current collector. After 800 cycles, it was found that the active material capacity decreases to 121 mAh/g. The results indicated that a part of the $LiCoO_2$ would have converted to an inactive form with cycling. Similar results were also obtained for the carbon electrode where the specific capacity decreases from 306 to 239 mAh/g after 800 cycles. Loss in capacity of $LiCoO_2$ and carbon with cycling can arise due to formation of either surface layers or conversion of active material to inactive form. Thus, next XRD material characterization studies were done on the electrodes after different cycles.

Fig. 14 presents the XRD patterns of the fully lithiated positive electrode from different cells. All the XRD patterns show a perfect crystalline structure with all peaks indicating hexagonal lattice [22]. From the XRD patterns it was found that peaks start to shift to higher 2θ values with cycling. This results in a variation in the lattice parameters '*a*' and '*c*' and hence a decrease in the *c*/*a* ratio with cycling. The table inside Fig. 14 gives the values of *c*/*a* ratio for the fresh $LiCoO_2$ material as well as the material taken from the cell cycled 150, 300 and 800 times. The decrease in the *c*/*a* ratio indicates a decrease in the Li stoichiometry with cycling.

Summarizing the results obtained for Sony 18650 cells, we could say that the rate capability of the cells continues to decrease with cycling and this decrease in rate capability can be attributed to increased resistance at both electrodes. Impedance measurements for both full and half-cells show an overall increase in the cell resistance with cycling. Charge/discharge studies on individual pellet electrodes show a reduced tendency for lithiation for both $LiCoO_2$ and carbon. XRD studies of the positive electrode up to 800 cycles shows a decrease in the Li stoichiometry with cycling.

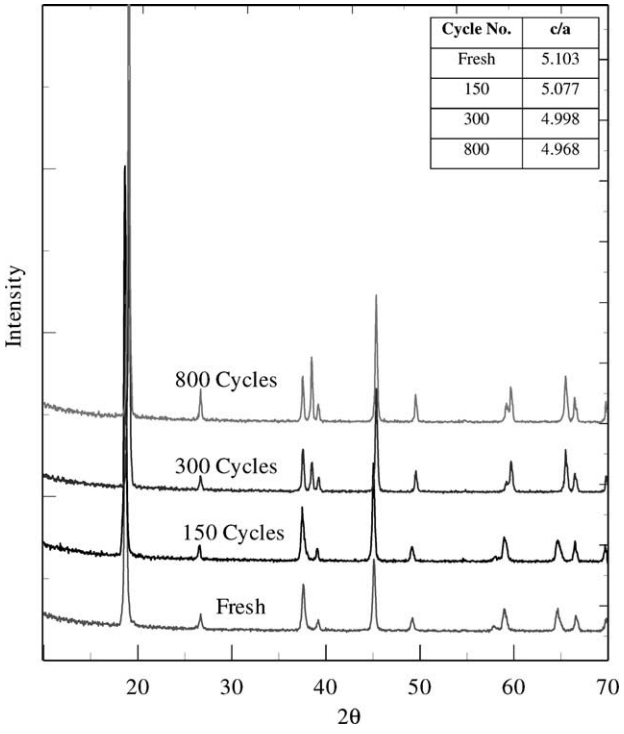

Fig. 14. XRD patterns of $LiCoO_2$ after different cycles and *c*/*a* ratio for the respective cycle numbers.

4. Conclusions

Capacity fade of Cell-Batt® Li-ion cells and Sony 18650 cells using non-stoichiometric spinel and $LiCoO_2$, respectively, as positive electrode material has been studied under several modes of charging. During cycling, the cells were opened at intermittent cycles and extensive material and electrochemical characterization was done on the active material at both electrodes.

Cycling studies were done for Cell-Batt® cell under several modes of charging namely charging the cell potentiostatically, CC–CV charging to several end potentials and CC–CV charging with different dc currents during the CC part. Cells charged to an end potential of 4.17 V gave better performance in terms of utilization and capacity loss with cycling when compared with cells charged to other values of end potentials. The cells charged with a direct current of 0.5 A during the CC charging gave better performance and less capacity fade of about 16% for 800 cycles of charge and discharge when compared with other charging rates. Impedance studies on spinel-based Li-ion cells show no significant increase in resistance at both electrodes with cycling. Low rate charge/discharge studies for positive and negative electrodes using T-cell shows that part of the capacity fade can be attributed to the change in lithiation capacity of the individual electrodes. XRD studies of spinel electrode reveal

the formation of an additional phase (λ-MnO_2) with cycling that leads to dissolution of Mn in the electrolyte, which could be the reason for decrease in lithiation capacity of positive electrode with cycling. Electrolyte oxidation due to overcharge causes acid formation as well as Mn dissolution that results in increased presence of Mn over the surface of carbon with cycling which could be attributed to decrease in specific capacity of negative electrode with cycling. Hence, capacity fade of the spinel-based Li-ion cells can be attributed to structural degradation at the cathode and loss of active materials at both electrodes due to electrolyte oxidation.

For Sony 18650 cells charging was done with CC–CV protocol with a charging current of 1 A and 4.2 V as the cut-off value and discharge current used 1 A. Capacity fade was found to be about 30% for 800 cycles of charge and discharge. Impedance measurements showed an overall increase in the cell resistance with cycling. The positive electrode resistance dominates during the entire cycling period. Similar to results obtained for Cell-Batt® cells, the specific capacity of both positive ($LiCoO_2$) and negative (carbon) electrodes continues to decrease with cycling. XRD studies of $LiCoO_2$ material taken from fresh as well as cycled cells shows a decrease in the Li stoichiometry with cycling. Thus, capacity fade in Sony Li-ion cells is attributed to oxidation of cathode ($LiCoO_2$) during overcharge and loss of both primary (Li^+) and secondary active material ($LiCoO_2$) during charging.

Acknowledgements

The authors are grateful for the financial support provided by National Reconnaissance Organization (NRO) under Contract no. NRO-00-C-0134.

References

[1] P. Arora, R.E. White, M. Doyle, J. Electrochem. Soc. 145 (1998) 3647.
[2] R. Fong, U. Von Sacken, J.R. Dahn, Studies of lithium intercalation into carbons using non-aqueous electrochemical cells, J. Electrochem. Soc. 137 (1990) 2009.
[3] Y. Ein-Eli, B. Markovsky, D. Aurbach, Y. Carmeli, H. Yamin, S. Luski, The dependence of the performance of Li/C intercalation anodes for Li-ion secondary batteries on the electrolyte solution composition, Electrochim. Acta 39 (1994) 2559.
[4] J.R. Dahn, E.W. Fuller, M. Obravae, U. Von Sacken, Thermal stability of Li_xCoO_2, Li_xNiO_2 and λ-MnO_2 and consequences for the safety of Li-ion cells, Solid State Ionics 69 (1994) 265.
[5] E. Peled, Fundamentals of lithium and lithium-ion electrode reactions in polymer and liquid electrolytes, Proc. Electrochem. Soc. 94-28 (1995) 1–15.
[6] E. Peled, Lithium stability and film formation in organic and inorganic electrolyte for lithium battery systems, in: J.P. Gabano (Ed.), Lithium Batteries, Academic Press, New York, 1983.
[7] E. Peled, D. Golodnitsky, G. Ardel, C. Menachem, D.B. Tow, V. Eshkenazy, The role of SEI in lithium and lithium-ion batteries, Mater. Res. Soc. Symp. Proc. 393 (1995) 209–221.
[8] M.C. Smart, B.V. Ratnakumar, S. Surampudi, Y. Wang, X. Zhang, B. Fultz, J. Electrochem. Soc. 146 (1999) 3963.
[9] R.J. Gummow, A. de Kock, M.M. Thackeray, Solid State Ionics 69 (1994) 59.
[10] J.M. Tarascon, W.R. McKinnon, F. Coowar, T.N. Bowmer, G. Amatucci, D. Guyomard, Synthesis conditions and oxygen stoichiometry effects on lithium insertion into the spinel $LiMn_2O_4$, J. Electrochem. Soc. 141 (1994) 1421.
[11] S.J. Wen, T.J. Richardson, L. Ma, K.A. Striebel, P.N. Ross Jr., E.J. Cairns, J. Electrochem. Soc. 143 (1996) L136.
[12] J.M. Tarascon, W.R. McKinnon, F. Coowar, T.N. Bowmer, G. Amatucci, D. Guyomard, Synthesis conditions and oxygen stoichiometry effects on lithium insertion into the spinel $LiMn_2O_4$, J. Electrochem. Soc. 141 (1994) 1421.
[13] D.H. Jang, Y.J. Shin, S.M. Oh, Dissolution of spinel oxides and capacity losses in 4 V $Li/Li_xMn_2O_4$ cells, J. Electrochem. Soc. 143 (1996) 2204.
[14] Y. Xia, Y. Zhou, M. Yoshio, Capacity fading on cycling of 4 V $Li/LiMn_2O_4$ cells, J. Electrochem. Soc. 144 (1997) 2593.
[15] D. Zhang, B.S. Haran, A. Durairajan, R.E. White, Y. Podrazhansky, B.N. Popov, J. Power Sources 91 (2000) 122.
[16] P. Ramadass, A. Durairajan, B.S. Haran, R.E. White, B.N. Popov, J. Electrochem. Soc. 149 (2001) A54.
[17] D. Aurbach, M.D. Levi, K. Gamulski, B. Markovsky, G.. Salitra, E. Levi, U. Heider, L. Heider, R. Oesten, J. Power Sources 81/82 (1999) 472.
[18] E. Wang, D. Ofer, W. Bowden, N. Iltchev, T. Moses, K. Brandt, J. Electrochem. Soc. 147 (2000) 4023.
[19] H. Huang, C.A. Vincent, P.G.. Bruce, J. Electrochem. Soc. 146 (1999) 3649.
[20] J. Cho, M.M. Thackeray, J. Electrochem. Soc. 146 (1999) 3577.
[21] J.C. Hunter, J. Solid State Chem. 39 (1981) 142.
[22] G.T.-K. Fey, V. Subramanian, J.-G. Chen, Electrochem. Commun. 3 (2001) 234.